Geophysical Research Letters

RESEARCH LETTER
10.1002/2018GL077004

Key Points:
- A parameterization scheme based on deep learning neural network is proposed for atmosphere-only typhoon forecast models
- The deep learning algorithm is designed to combine information from historical data and the target typhoon
- The scheme based on the deep learning algorithm achieves an equivalent representation as the fully coupled model

Correspondence to:
J. Wei,
junwei@pku.edu.cn

Citation:
Jiang, G.-Q., Xu, J., & Wei, J. (2018). A deep learning algorithm of neural network for the parameterization of typhoon-ocean feedback in typhoon forecast models. *Geophysical Research Letters*, *45*. https://doi.org/10.1002/2018GL077004

Received 3 JAN 2018
Accepted 21 MAR 2018
Accepted article online 26 MAR 2018

©2018. The Authors.
This is an open access article under the terms of the Creative Commons Attribution-NonCommercial-NoDerivs License, which permits use and distribution in any medium, provided the original work is properly cited, the use is non-commercial and no modifications or adaptations are made.

A Deep Learning Algorithm of Neural Network for the Parameterization of Typhoon-Ocean Feedback in Typhoon Forecast Models

Guo-Qing Jiang[1,2], Jing Xu[3], and Jun Wei[1]

[1]Department of Atmospheric and Oceanic Sciences, Peking University, Beijing, China, [2]Department of Earth, Atmospheric and Planetary Sciences, Massachusetts Institute of Technology, Boston, MA, USA, [3]State Key Laboratory of Severe Weather, Chinese Academy of Meteorological Sciences, Beijing, China

Abstract Two algorithms based on machine learning neural networks are proposed—the shallow learning (S-L) and deep learning (D-L) algorithms—that can potentially be used in atmosphere-only typhoon forecast models to provide flow-dependent typhoon-induced sea surface temperature cooling (SSTC) for improving typhoon predictions. The major challenge of existing SSTC algorithms in forecast models is how to accurately predict SSTC induced by an upcoming typhoon, which requires information not only from historical data but more importantly also from the target typhoon itself. The S-L algorithm composes of a single layer of neurons with mixed atmospheric and oceanic factors. Such a structure is found to be unable to represent correctly the physical typhoon-ocean interaction. It tends to produce an unstable SSTC distribution, for which any perturbations may lead to changes in both SSTC pattern and strength. The D-L algorithm extends the neural network to a 4 × 5 neuron matrix with atmospheric and oceanic factors being separated in different layers of neurons, so that the machine learning can determine the roles of atmospheric and oceanic factors in shaping the SSTC. Therefore, it produces a stable crescent-shaped SSTC distribution, with its large-scale pattern determined mainly by atmospheric factors (e.g., winds) and small-scale features by oceanic factors (e.g., eddies). Sensitivity experiments reveal that the D-L algorithms improve maximum wind intensity errors by 60–70% for four case study simulations, compared to their atmosphere-only model runs.

Plain Language Summary Forecasting accuracy with respect to storm track and intensity are two important factors for evaluating typhoon models. While 24-h forecast errors of typhoon track have steadily improved to an order of 50 km, the prediction of typhoon intensity has remained one of the major challenges during the last decade. In this study, two algorithms based on machine-learning neural networks are proposed-the shallow learning (S-L) and deep learning (D-L) algorithms-that can potentially be used in atmosphere-only typhoon forecast models to provide flow-dependent typhoon-induced sea surface temperature cooling (SSTC) for improving typhoon predictions.

1. Introduction

Forecasting accuracy with respect to storm track and intensity are two important factors for evaluating typhoon models. While 24-h forecast errors of typhoon track have steadily improved to an order of 50 km, the prediction of typhoon intensity has remained one of the major challenges during the last decade (Gall et al., 2013; Ginis, 2002). To improve typhoon intensity forecasts, aside from better resolving the dynamics of typhoon inner core and understanding its multiscale interactions, the oceanic boundary layer might also play a significant role. Large quantities of heat and momentum exchange occur at the typhoon-ocean interface that modify the typhoon structure and intensity. Strong typhoon winds transfer momentum fluxes into the ocean, producing significant sea surface temperature cooling (SSTC). This typhoon-induced SSTC acts as a negative feedback, which modifies the storm's dynamical and thermal structure near ocean surface through moisture flux (Anthes & Chang, 1978; Emanuel, 2003). Previous studies have confirmed that SSTC strength and structure can be affected by typhoon intensity, size, and translation speed (Anthes & Chang, 1978; DeMaria & Kaplan, 1994; Emanuel et al., 2004; Price 1981; Zhu & Zhang, 2006). In particular, a large SSTC of greater than 2.5 °C is considered not conducive to typhoon strengthening (Emanuel, 1999) and may even lead to typhoon weakening (Lin et al., 2008; Schade & Emanuel, 1999).

In order to include the effects of sea surface temperature (SST) in typhoon forecast models, most previous studies have tended to use fixed SST with time (Braun, 2002; Chen et al., 2011) or specified satellite-

derived SST as ocean boundary conditions (Chelton, 2005; Vincent et al., 2012; Zhu & Zhang, 2006). However, these specified SSTs from climatological data or satellite images fail to present a flow-dependent SSTC and its feedback. Most importantly, the satellite data cannot provide "future" SSTC information for an upcoming typhoon, which leads to a warm bias for typhoon forecasts. On the other hand, some operational models have developed air-sea fully coupled models for typhoon prediction (Bender et al., 1993, 2007; Chen & Gopalakrishnan, 2015; Gopalakrishnan et al., 2011; Warner et al., 2010). Although these coupled models are able to simulate the flow-dependent SSTC, unlike uncoupled atmosphere-only models, such as the Advanced Research version of the Weather Research and Forecasting (WRF) model (WRF-ARW), which has long been widely used in the weather prediction community, fully coupled models are computationally expensive and only just starting to become publicly available. From a practical point of view, it remains challenging for the typhoon community to replace existing operational forecast systems with coupled models at this stage (Wei et al., 2017).

Developing a prognostic SSTC parameterization algorithm for typhoon forecast models to include the effects of SSTC has been an aim since the 1980s (Black, 1993). The WRF model has been implemented with simplified ocean models, such as a 1-D ocean mixed layer model (Davis et al., 2008; Pollard et al., 1973) and the 3D-PWP model (Price, 2009). Zeng and Beljaars (2005) incorporated a parameterization scheme in the WRF model, accounting for the effects on typhoons of daily SST variations. Based on ocean temperature equations and neural network methods, one of our previous studies proposed two algorithms to estimate typhoon-induced SSTC (Wei et al., 2017). This and the other studies mentioned confirm that the WRF model with an SSTC scheme can significantly improve WRF-only simulations of typhoon intensity. However, in any such SSTC scheme, the efficiency of the algorithm eventually relies on its weighting function, which is given either empirically or by fitting and training from historical typhoon information. Wei et al. (2017) suggested that if the training set from historical typhoons is not diverse enough, SSTC neural network algorithms trained by such a data set might not be able to predict reasonably well an upcoming typhoon that is not included in the training set. Thus, accurately predicting the SSTC of an upcoming storm relies not only on general information from historical typhoon data but also on specific information from the target typhoon. Obviously, this task cannot be achieved by using simplified ocean schemes with historical data only (Pollard et al, 1973; Zeng & Beljaars, 2005), or linear shallow learning (S-L) neural network algorithms (Wei et al., 2017). Instead, we propose a nonlinear deep learning (D-L) neural network algorithm, with the aim to combine historical data and the target typhoon for better resolving typhoon-induced SSTC feedback in the WRF model.

2. Model, Data, and Methods

2.1. Model and Data

Simulations from an air-sea fully coupled model are used as reference for assessing the parameterization schemes. The coupled model adopts version 3.6.1 of WRF-ARW (Skamarock et al., 2008) as the atmospheric component, the Regional Oceanic Modeling System (ROMS) (Shchepetkin & McWilliams, 2005) as the oceanic component, and OASIS3 as the coupler (Wei, Malanotte-Rizzoli, et al., 2014; Wei, Wang, et al., 2014). The model setup follows that used by Wei et al. (2017), wherein detailed information on the coupled model configuration can be found.

Three nested domains are adopted in WRF, with resolutions of 2 km, 6 km, and 18 km, respectively. The external domain is fixed, from 105°E to 160°E and 5°N to 45°N, and the two internal domains use storm-following grids. The same external domain is adopted in ROMS as in WRF, with a horizontal resolution of 18 km, initialized and forced by global HYbrid Coordinate Ocean Model (HYCOM) reanalysis data. The proposed SSTC algorithms are implemented in WRF to assess their effectiveness. Three sets of experiments (coupled model, WRF-only, and WRF-SSTC) are carried out using the same WRF-ROMS coupled model framework, with air-sea flux exchanges switched on/off. The WRF-only experiment uses satellite SST as its ocean boundary condition, and WRF-SSTC uses SSTs predicted by the neural network algorithms.

The data used to train the weighting coefficients in the algorithms can be divided into atmospheric and oceanic variables. The intensity and track information of typhoons are from the best track data provided by the Japan Meteorological Agency (JMA, http://www.jma.go.jp/jma/indexe.html). For the oceanic data, the Sea Surface Height (SSH) is from the Archiving, Validation, and Interpretation of

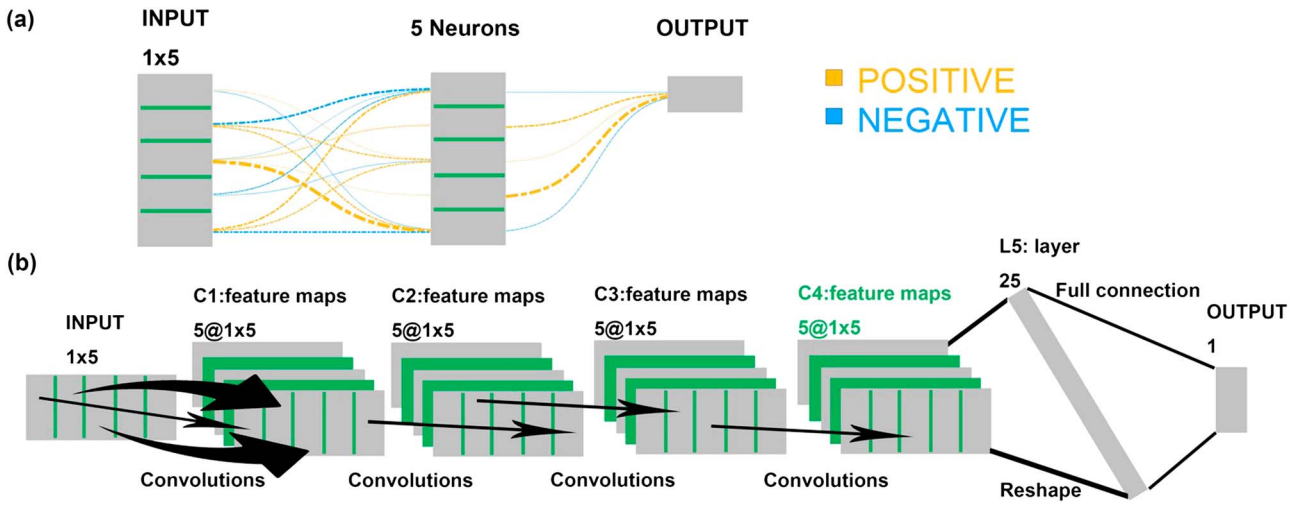

Figure 1. Schematic representations of the neural networks: (a) three-layer structure of the S-L neural network; (b) multilayer structure of the D-L neural network. The blue/yellow dashed lines in the S-L algorithm represent negative/positive weighting coefficients, with the width of each line indicating its weight.

Satellite Oceanographic data set (http://www.aviso.oceanobs.com), with a resolution of 0.25° × 0.25°; the subsurface temperature at a depth of 100 m (T_{100m}) is from the HYCOM reanalysis, which provides global oceanic reanalysis data at a resolution of 1/12° from 1992 to the present day (http://hycom.org/dataserver/glb-reanalysis); and the SST maps are from the Tropical Rainfall Measuring Mission Microwave Imager, which provides cloud-penetrating daily SST data (http://pmm.nasa.gov/TRMM) at a resolution of 0.25° × 0.25°.

2.2. S-L and D-L Neural Network Algorithms

Wei et al. (2017) introduced a simple S-L neural network for a case study of typhoon Soulik (2013). This neural network is based on a back-propagation algorithm (Rummelhart, 1986), which includes three layers: the input layer, the hidden layer, and the output layer (Figure 1a). The input layer consists of five variables: 10-m winds ($U10$ and $V10$), T_{100m}, SSH, and SST. The hidden layer consists of five neurons, each of which is a linear combination of the input variables. The output layer is the SSTC, calculated by a linear combination of the five neurons. The S-L algorithm can be presented as follows:

$$n = f\left(a\times\begin{bmatrix} U10 \\ V10 \\ \mathrm{SST0} \\ \mathrm{SSH0} \\ T_{100m} \end{bmatrix} + b\right) \tag{1}$$

$$\mathrm{SSTC} = f(c\times n + d) \tag{2}$$

where a and b are weights connecting the input variables to the neurons n; $f(n) = 2/(1 + e^{-2n}) - 1$, which performs a nonlinear normalization of n to [0,1]; and c and d in equation (2) connect the neurons to the output SSTC. Readers are referred to Wei et al. (2017) for a detailed description of the S-L algorithm and its learning process.

The D-L algorithm is based on a convolutional neural network proposed by LeCun et al. (1998), with the same input-hidden-output structure as the S-L algorithm, but involving multiple layers of neurons (Figure 1b). The extended hidden layer consists of four sublayers, each of which contains five independent feature maps. The D-L algorithm can be written as follows:

$$N_1 = f(a_1 \times [U10 \;\; V10 \;\; SST0 \;\; SSH0 \;\; T_{100m}] + b_1) \tag{3}$$

$$N_k = f(a_k \times N_{k-1} + b_k) \;\; (k = 2, \;\; 3, \;\; 4) \tag{4}$$

$$SSTC = f(c \times N_4 + d) \tag{5}$$

where N_k represents the 4×5 neuron matrix at the k sublayer; in equation (3), N_1 connects the inputs to the first sublayer neurons; and $N_{k\,=\,2\text{–}4}$ is calculated by a combination of the neurons from the previous sublayer ($N_{k\,-\,1}$), with a nonlinear function $f(x) = 1/(1 + e^{-x})$ and weighting matrices a_k and b_k. Note that both the S-L and D-L algorithms are trained by the same data set.

3. Typhoon-Induced SSTC Distribution

3.1. Observed and Simulated Typhoon-Induced SSTC

Figure 2 compares the observed and simulated (coupled model) SSTC of four typhoons, separately: Soulik, Neoguri, Halong, and Muifa. In general, the coupled model represents the observed SSTC patterns for all cases reasonably well. The model also reproduces the storm tracks and their intensity quite well, as compared to the best track observations provided by the JMA. Figures 2c, 2f, 2i, and 2l show composite maps of model transient SSTC snapshots at an interval of 3 hr during a specific period, marked by the black boxes in Figures 2b, 2e, 2h, and 2k. As shown, all cases demonstrate a crescent-shaped SSTC distribution, which is characterized by stronger cooling on the right-rear quadrant of the track but weaker cooling on the left and near the storm center. Note that the black boxes in Figures 2b, 2e, 2h, and 2k indicate the specific period for each typhoon case, for which the storm is moving toward different directions. We see that the crescent-shaped SSTC is rotating with the storm tracks, indicated by the dashed arrows in Figures 2c, 2f, 2i, and 2l, with ~10° for Soulik, ~45° for Neoguri, ~90° for Halong, and ~120° for Muifa. This indicates that the crescent-shaped SSTC might be a common feature for all four cases, and its orientation generally follows the moving direction of each typhoon. Case study simulations with another 17 typhoons confirm this track-following SSTC distribution (not shown).

The purpose of SSTC schemes is to predict the SSTC induced by an upcoming target typhoon accurately and provide the typhoon model with SST information at every time step. Therefore, the key to a robust SSTC scheme is being able to reproduce the transient crescent-shaped SSTC (the common feature), as well as its orientation relative to the target typhoon track. In this sense, the common crescent-shaped SSTC can be learned from the historical data, but its orientation must be linked to the target typhoon. As storm may change its track all the time, in order to resolve the common SSTC distribution, we first rotate all input data to the horizon (0°, referred to as the west). Then, the horizontal crescent-shaped SSTC is rotated back to the actual angle for each typhoon, before it is used in the WRF model.

3.2. SSTC Estimated From the S-L and D-L Algorithms

Wei et al. (2017) suggested that although the S-L algorithm is able to capture the general SSTC pattern, the SSTC is highly unstable, for which any perturbations of inputs will change its distribution. To resolve this problem, a D-L algorithm is developed in this study, involving a more complex and sufficient structure of neurons in the hidden layer. As shown in Figure 1b, a 4×5 neural network is used, containing a total of 100 neurons. It is found that although the neurons do not necessarily resolve physical processes, the more neurons involved, the better the resultant SSTC pattern obtained. Except for adding more neurons, the major difference between the S-L and D-L algorithms is that in the D-L algorithm, the input atmospheric and oceanic variables are assigned separately to different layers of neurons (black arrows in Figure 1b). By doing so, the atmospheric and oceanic information is transferred independently toward the output SSTC, so that the machine learning is able to determine which variables (atmospheric or oceanic) are important to shape the resultant SSTC pattern and strength. It is found that neurons with mathematically mixed atmospheric/oceanic variables cannot represent correctly the physical typhoon-ocean interaction.

A set of sensitivity experiments are used to examine the S-L and D-L algorithms. In the ocean-perturbed experiment, we artificially impose a subsurface cold anomaly in the oceanic variable T_{100m}. The atmospheric

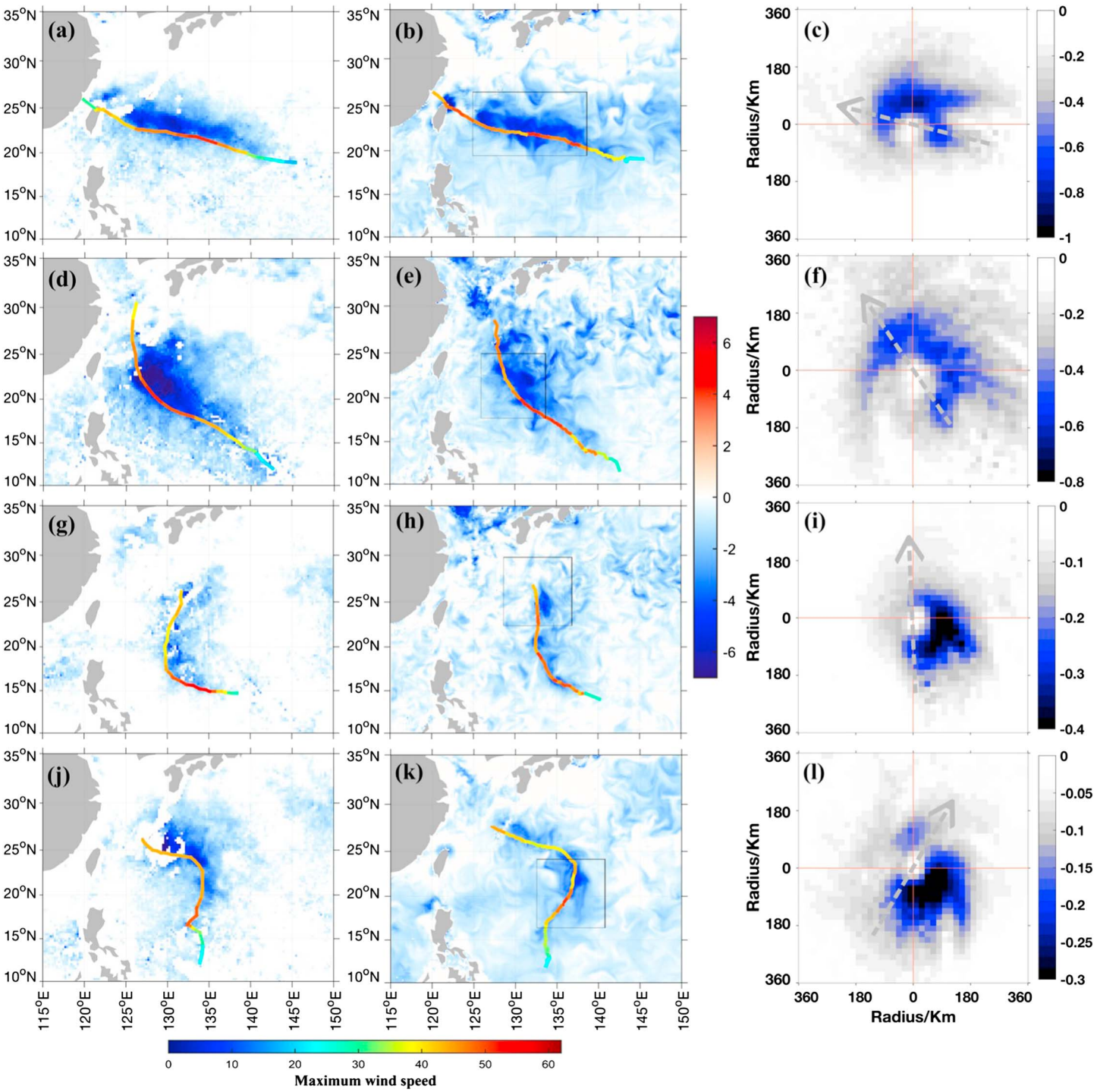

Figure 2. Sea surface temperature cooling from observations (a, d, g, and j) and the coupled model (b, e, h, and k) for four typhoon cases: (a, b) Soulik; (d, e) Neoguri; (g, h) Halong; and (j, k) Muifa. (c, f, i, and l) Composite SSTC maps of 3-hr transient snapshots for each case. The gray dashed arrows indicate the storm's moving direction.

variables ($\overline{U10}$ and $\overline{V10}$) and SST0 are kept the same as in the control experiment. The purpose of this test is to examine the two algorithms in response to a scenario that a typhoon is propagating over a mesoscale cold-core eddy. For the atmosphere-perturbed experiment, the wind field is rotated 90° clockwise, the purpose of which is to examine the SSTC orientation in response to the typhoon's moving direction.

Figure 3 shows SSTC snapshots obtained from the control and perturbed experiments. As expected, in the control test, the D-L algorithm obtains a more organized crescent-shaped SSTC distribution than the S-L algorithm (Figures 3a and 3b). The SSTC from the S-L algorithm indicates that the five neurons connect to all the atmospheric/oceanic inputs, which combine together to produce an irregular-shaped SSTC. In contrast, the D-L algorithm separates the input atmospheric and oceanic variables with different layers of neurons, and therefore, the resultant crescent-shaped SSTC is mainly determined by the wind fields. For the ocean-perturbed test, SSTC from the S-L algorithm becomes stronger within the box due to the presence of the cold eddy, but its distribution changes as well (Figure 3c). Given that all input variables are combined to produce the SSTC, any perturbations of the input variables may lead to changes in SSTC distribution and strength. In contrast, the SSTC strength from the D-L algorithm is enhanced within the cold-core box only, but it keeps the same distribution as the control test (Figure 3d). With the D-L algorithm, the large-scale SSTC pattern responds to atmospheric variables and its small-scale features to the oceanic variables. This is well supported by the atmosphere-perturbed test, in which the rotated wind field can only affect the SSTC orientation without changing its cooling structure and strength (Figures 3e and 3f). Considering that the transient SSTC orientation evolves with the typhoon's moving direction, obviously the D-L algorithm is more effective in producing a stable crescent-shaped SSTC than the S-L algorithm. The crescent-shaped SSTC can then be rotated according to the target typhoon track before it is implemented into the WRF model.

4. WRF Simulations With the S-L and D-L Algorithms

The S-L and D-L algorithms are implemented in the WRF model to provide SST boundary conditions for all four typhoon simulations. The initial oceanic variables are taken from HYCOM reanalysis data and assumed unchanged during the typhoon simulations. Three simulations are carried out, using the S-L algorithm and the D-L algorithms with/without rotation. As shown in Figure 4, the three algorithms are able to produce a reasonable SSTC pattern with rightward bias compared with the coupled model (Figures 2b, 2e, 2h, and 2k). In particular, the S-L algorithm (Figures 4a, 4d, 4g, and 4j) obtains a relatively stronger SSTC. The SSTC pattern of the D-L algorithm appears to be quite similar to that of the D-L rotated algorithm in the case of Soulik, but notable differences are apparent for Halong and Muifa. Specifically, the D-L rotated algorithm works better in the case of Muifa, when Muifa turns from northeast toward the northwest (Figure 4l).

Figure 5 shows the WRF simulations of four cases with the S-L algorithm and D-L algorithm with rotation, referred to as the WRF-S-L and WRF-D-L-R, respectively. For comparison, the observed typhoon intensity from JMA records as well as the WRF-only and WRF-ROMS coupled experiments are also included. The WRF-only experiment uses a prescribed SST condition from Tropical Rainfall Measuring Mission Microwave Imager satellite data and thereby contains no ocean cooling feedback. Due to the warm bias of the prescribed SST, it appears that the WRF-only experiments overestimate the typhoon intensity for all four cases during the typhoon decaying phase, as compared to the observed one. The coupled model generally achieves a better typhoon intensity by using the ocean model to resolve a flow-dependent SST condition. On the other hand, both the WRF-S-L and WRF-D-L-R experiments effectively inhibit the overly rapid intensification of four typhoons in the WRF-only experiment, indicating that the SSTC feedback plays an important role in modeling the typhoon intensity. Among the S-L and D-L-R algorithms, the S-L generally underestimates the typhoon intensity, as it produces a stronger SSTC. In general, the WRF-D-L-R experiments obtain the best result among all the schemes, as compared to the coupled model.

Table 1 shows the mean absolute errors (MAEs) of maximum wind intensity and SST of all sensitivity experiments, calculated against the results from the coupled model. We see that the WRF-only experiments for all cases show the largest MAEs, without considering the SSTC effect. Taking Soulik as an example, the MAE of max wind intensity is 5.3 ms^{-1}, while in the experiments with S-L, D-L, and D-L-R algorithms, the MAE decreases to 2.5, 1.3, and 1.2 ms^{-1}, respectively. As shown, the D-L-R algorithm overall shows the best performance, which achieves significant improvement of MAEs by 77% (Soulik), 65% (Neoguri), 67% (Halong), and 63% (Muifa), respectively. As expected, the D-L-R algorithm also significantly improve the MAEs of SST.

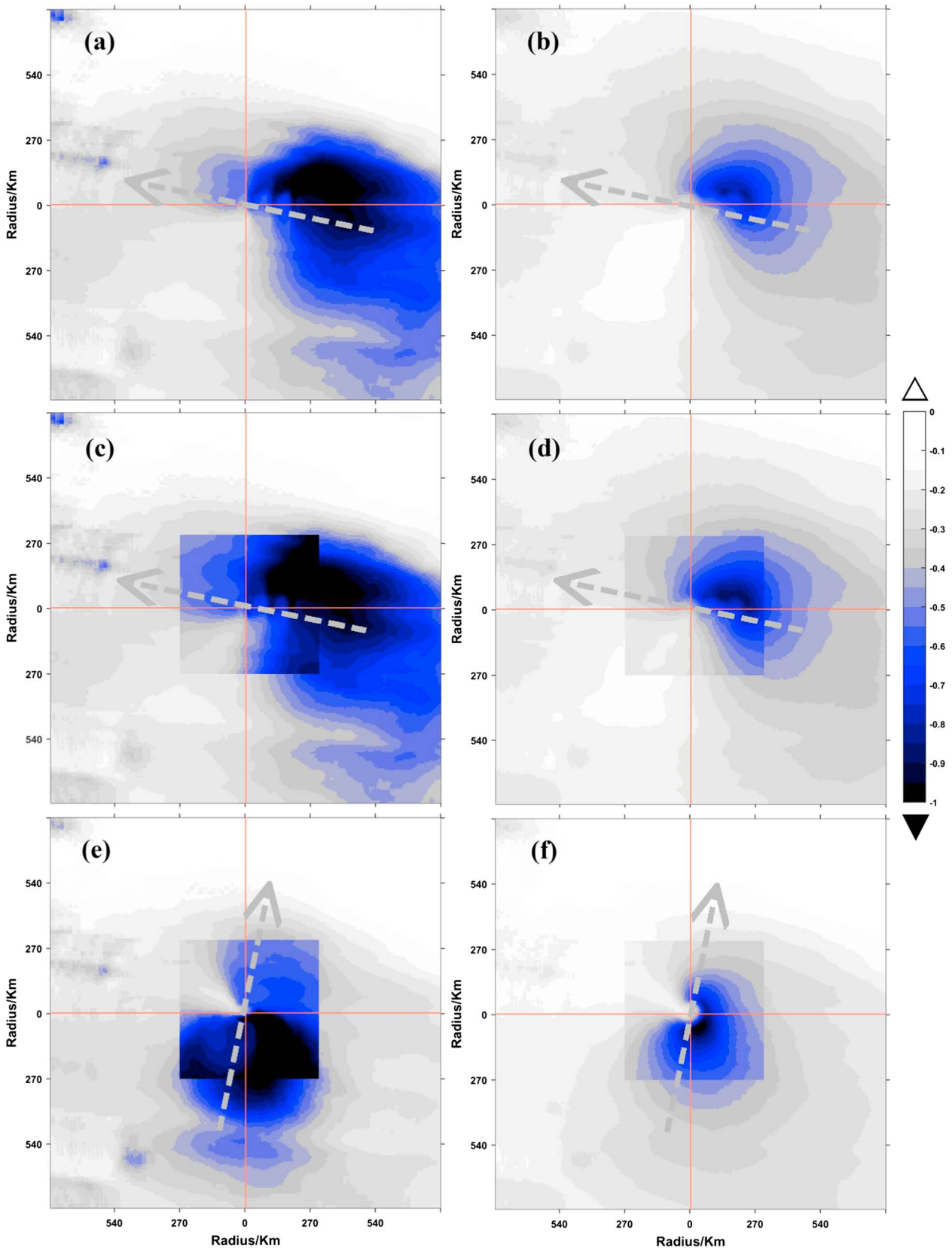

Figure 3. The sea surface temperature cooling distribution estimated by the shallow learning and deep learning algorithms in the (a, b) control experiment, (c, d) oceanic-perturbation experiment, and (e, f) atmospheric-perturbation experiment. The gray dashed arrows indicate the storm's moving direction.

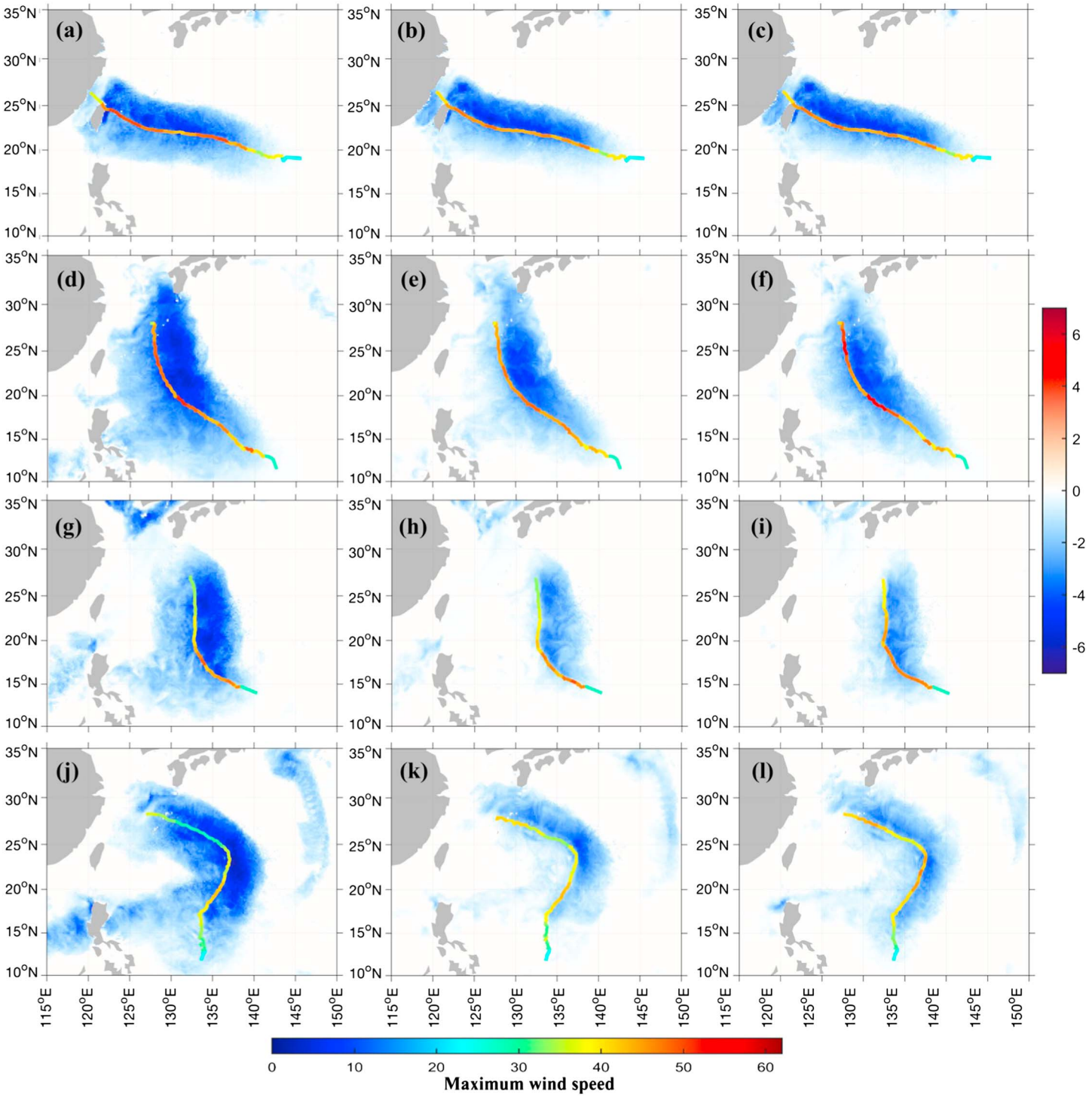

Figure 4. Implementation of the shallow learning algorithm (a, d, g, and j), deep learning algorithm (b, e, h, and k), and deep learning rotated algorithm (c, f, i, and l) in the Weather Research and Forecasting model for four typhoon cases: (a–c) Soulik; (d–f) Neoguri; (g–i) Halong; and (j–l) Muifa.

5. Summary and Discussion

A D-L neural network is proposed in this study and applied to a typhoon forecast model to parameterize typhoon-ocean interactions. The D-L algorithm is designed to achieve the transient crescent-shaped SSTC induced by typhoons, first proposed by Black (1993), for which the atmospheric and oceanic input

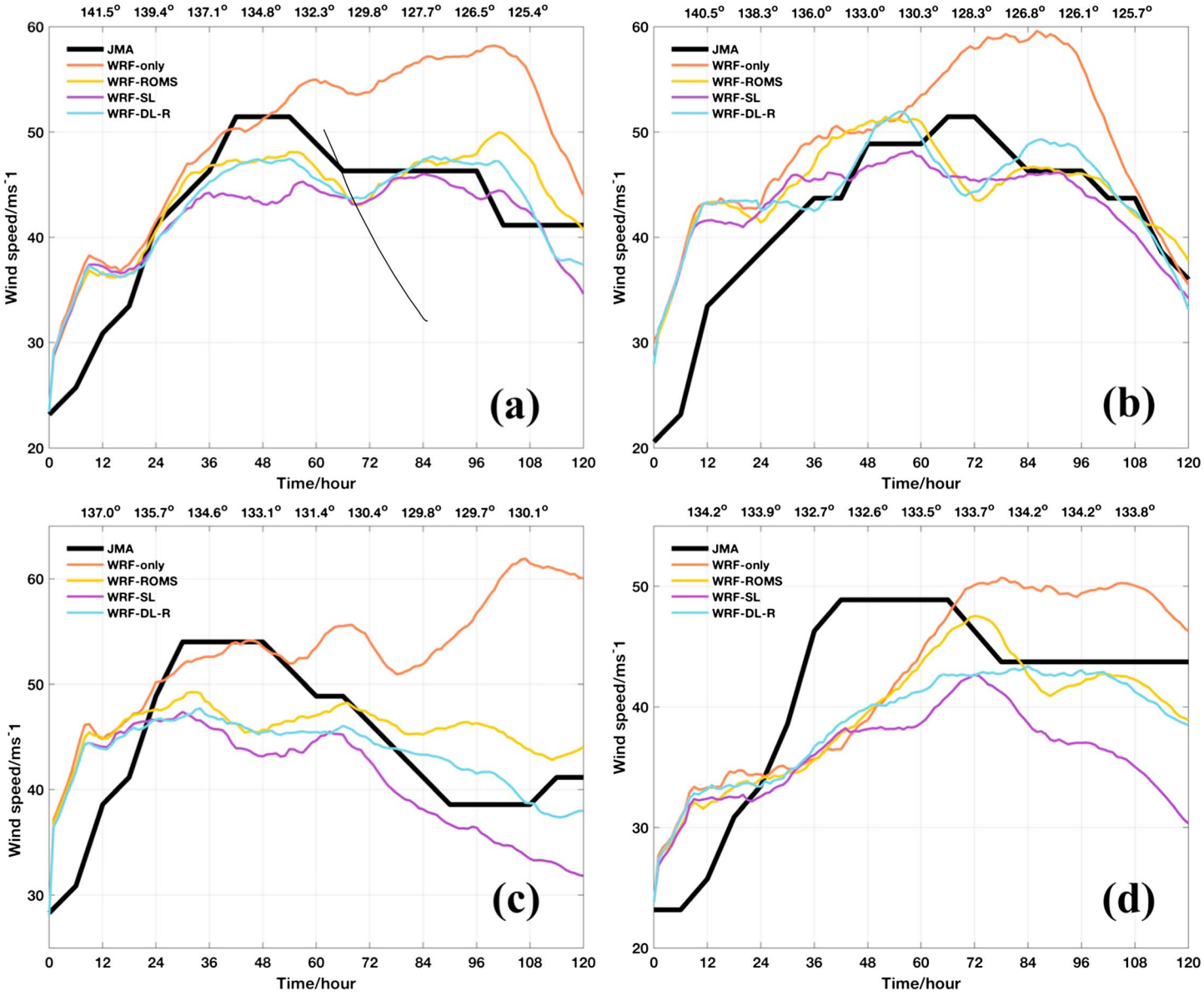

Figure 5. Comparison of simulated maximum wind speed for (a) Soulik, (b) Neoguri, (c) Halong, and (d) Muifa using Weather Research and Forecasting (WRF) with shallow learning (S-L) and deep learning with rotation (D-L-R) algorithms. Results from the Japan Meteorological Agency (JMA) records, WRF-only, and WRF-Regional Oceanic Modeling System (ROMS) coupled model are also included for comparison. The locations of the storm center corresponding to simulation time are marked on top of each figure.

Table 1
MAEs (ms^{-1}/°C) of Max Wind Intensity (WND) and SST

Case name (year)	WRF-only (WND/SST)	WRF-S-L (WND/SST)	WRF-D-L (WND/SST)	WRF-D-L-R (WND/SST)
Soulik (2013)	5.3/1.96	2.5/0.78	1.3/0.74	1.2/0.72
Neoguri (2014)	4.6/2.00	2.1/1.05	2.0/0.66	1.6/0.57
Halong (2014)	7.1/1.83	4.8/1.32	4.4/0.97	2.3/0.77
Muifa (2011)	3.3/1.56	3.4/1.21	2.6/0.93	1.2/0.77

Note. The mean absolute errors (MAEs) of all experiments are calculated against the results from the coupled model. WRF = Weather Research and Forecasting; SST = sea surface temperature; WRF-S-L = WRF with shallow learning algorithm; WRF-D-L = WRF with deep learning algorithm; WRF-D-L-R = WRF with deep learning with rotation algorithm.

variables are separated to determine the SSTC structure and strength, respectively. Note that it is not easy to extract the crescent-shaped SSTC distribution from satellite-derived SST images because of the poor temporal resolution (1–3 days), but such an SSTC pattern is resolved well by the WRF-ROMS coupled model and is consistent with aircraft-based observations (Black et al., 2007). The results of four typhoon cases from the coupled model show that stronger (weaker) typhoons result in larger (smaller) crescent-shaped SSTC, which rotates following the typhoon's moving direction.

To resolve the typhoon-induced SSTC, three algorithms are then developed on the basis of machine learning neural networks (namely, the S-L, D-L, and D-L rotated algorithms), which can potentially be used in atmosphere-only weather forecast models to provide flow-dependent typhoon-induced SSTC for modeled typhoons. The S-L algorithm contains one layer of five neurons, and the D-L algorithm is extended to a 4×5 neuron matrix. To assess their effectiveness, the algorithms are trained offline using atmospheric and oceanic outputs from a fully coupled air-sea model that simulates typhoon Soulik (2013) reasonably well. The algorithms and the trained weighting coefficients are then implemented into the WRF model to estimate the typhoon-induced SSTC, which is used to provide a cooling feedback to the model typhoon.

The results show that the S-L algorithm is directly related to a linear combination of all input variables. Any perturbations of the inputs may lead to changes in SSTC structure and strength. The D-L algorithm separates the atmospheric and oceanic variables with different layers of neurons, such that a more stable SSTC can be resolved in terms of its structure and strength. A set of sensitivity tests with perturbed atmospheric and ocean variables reveal that the design of the D-L neural network is necessary for the SSTC algorithm to resolve the cooling position and amplitude efficiently, both of which may have important effects in modeling the typhoon intensity and structure. The D-L rotated algorithm combines the common SSTC distribution and moving direction of the target typhoon and therefore achieves an equivalent representation to the coupled model. The advantage of the D-L algorithm over the S-L one is that it capture well the crescent-shaped SSTC pattern. This pattern is found to be a fundamental feature extracted from historical typhoon sets and therefore can be used to predict the upcoming typhoon, even not included in the training set.

Acknowledgments
This work was supported by the National Basic Research and Development Project (973 program) of China under contract 2016YFA0202704 and 2015CB452805, the Basic Research Fund of CAMS 2016Z003, National Natural Science Foundation of China (41476008 and 41576018), and the Strategic Priority Research Program of the Chinese Academy of Sciences (XDA11010303). We thank the HYCOM data set (http://hycom.org/dataserver/glb-reanalysis) for providing subsurface temperature fields, Tropical Rainfall Measuring Mission (TRMM, http://pmm.nasa.gov/TRMM) for providing SST data, the Japan Meteorological Agency (JMA, http://www.jma.go.jp/jma/indexe.html) for providing typhoon information, and the Archiving, Validation, and Interpretation of Satellite Oceanographic (AVISO) data set (http://www.aviso.oceanobs.com) for providing SSH data.

References

Anthes, R. A., & Chang, S. W. (1978). Response of the hurricane boundary layer to changes of sea surface temperature in a numerical model. *Journal of the Atmospheric Sciences*, *35*(7), 1240–1255. https://doi.org/10.1175/1520-0469(1978)035%3C1240:ROTHBL%3E2.0.CO;2

Bender, M. A., Ginis, I., & Kurihara, Y. (1993). Numerical simulations of tropical cyclone-ocean interaction with a high-resolution coupled model. *Journal of Geophysical Research*, *98*(D12), 23,245–23,263. https://doi.org/10.1029/93JD02370

Bender, M. A., Ginis, I., Tuleya, R., Thomas, B., & Marchok, T. (2007). The operational GFDL coupled hurricane-ocean prediction system and a summary of its performance. *Monthly Weather Review*, *135*(12), 3965–3989. https://doi.org/10.1175/2007MWR2032.1

Black, P. G. (1993). Ocean temperature changes induced by tropical cyclones (PhD thesis) (278 pp.). Department of Meteorology, Pennsylvania State University.

Black, P. G., D'Asaro, E. A., Sanford, T. B., Drennan, W. M., Zhang, J. A., French, J. R., et al. (2007). Air–sea exchange in hurricanes: Synthesis of observations from the coupled boundary layer air–sea transfer experiment. *Bulletin of the American Meteorological Society*, *88*(3), 357–374. https://doi.org/10.1175/BAMS-88-3-357

Braun, S. A. (2002). A cloud-resolving simulation of Hurricane Bob (1991): Storm structure and eyewall buoyancy. *Monthly Weather Review*, *130*(6), 1573–1592. https://doi.org/10.1175/1520-0493(2002)130%3C1573:ACRSOH%3E2.0.CO;2

Chelton, D. B. (2005). The impact of SST specification on ECMWF surface wind stress fields in the eastern tropical Pacific. *Journal of Climate*, *18*(4), 530–550. https://doi.org/10.1175/JCLI-3275.1

Chen, H., & Gopalakrishnan, S. G. (2015). A study on the asymmetric rapid intensification of Hurricane Earl (2010) using the HWRF system. *Journal of the Atmospheric Sciences*, *72*(2), 531–550. https://doi.org/10.1175/JAS-D-14-0097.1

Chen, H., Zhang, D., Carton, J., & Atlas, R. (2011). On the rapid intensification of Hurricane Wilma (2005). Part I: Model prediction and structural changes. *Weather Forecasting*, *26*(6), 885–901. https://doi.org/10.1175/WAF-D-11-00001.1

Davis, C., Wang, W., Chen, S. S., Chen, Y., Corbosiero, K., DeMaria, M., et al. (2008). Prediction of landfalling hurricanes with the Advanced Hurricane WRF model. *Monthly Weather Review*, *136*(6), 1990–2005. https://doi.org/10.1175/2007MWR2085.1

DeMaria, M., & Kaplan, J. (1994). Sea surface temperature and the maximum intensity of Atlantic tropical cyclones. *Journal of Climate*, *7*(9), 1324–1334. https://doi.org/10.1175/1520-0442(1994)007%3C1324:SSTATM%3E2.0.CO;2

Emanuel, K., DesAutels, C., Holloway, C., & Korty, R. (2004). Environmental control of tropical cyclone intensity. *Journal of the Atmospheric Sciences*, *61*(7), 843–858. https://doi.org/10.1175/1520-0469(2004)061%3C0843:ECOTCI%3E2.0.CO;2

Emanuel, K. A. (1999). Thermodynamic control of hurricane intensity. *Nature*, *401*(6754), 665–669. https://doi.org/10.1038/44326

Emanuel, K. A. (2003). A similarity hypothesis for air-sea exchange at extreme wind speeds. *Journal of the Atmospheric Sciences*, *60*(11), 1420–1428. https://doi.org/10.1175/1520-0469(2003)060%3C1420:ASHFAE%3E2.0.CO;2

Gall, R., Franklin, J., Marks, F., Rappaport, E. N., & Toepfer, F. (2013). The hurricane forecast improvement project. *Bulletin of the American Meteorological Society*, *94*(3), 329–343. https://doi.org/10.1175/BAMS-D-12-00071.1

Ginis, I. (2002). Tropical cyclone-ocean interactions. *Advances in Fluid Mechanisms*, *33*, 83–114.

Gopalakrishnan, S. G., Marks, F. Jr., Zhang, X., Bao, J. W., Yeh, K. S., & Atlas, R. (2011). The experimental HWRF system: A study on the influence of horizontal resolution on the structure and intensity changes in tropical cyclones using an idealized framework. *Monthly Weather Review*, *139*(6), 1762–1784. https://doi.org/10.1175/2010MWR3535.1

LeCun, Y., Bottou, L., Bengio, Y., & Haffner, P. (1998). Gradient-based learning applied to document recognition. *Proceedings of the IEEE*, *86*(11), 2278–2324.

Lin, I. I., Wu, C., Pun, I., & Ko, D. (2008). Upper-ocean thermal structure and the western North Pacific category 5 typhoons. Part I: Ocean features and the category 5 typhoons' intensification. *Monthly Weather Review*, *136*(9), 3288–3306. https://doi.org/10.1175/2008MWR2277.1

Pollard, R. T., Rhines, P. B., & Thompson, R. O. R. Y. (1973). The deepening of the wind-mixed layer. *Journal of Geophysical Fluid Dynamics*, *3*, 381–404.

Price, J. F. (1981). Upper ocean response to a hurricane. *Oceanography*, *11*, 153–175.

Price, J. F. (2009). Metrics of hurricane-ocean interaction: Vertically-integrated or vertically-averaged ocean temperature. *Ocean Science Discussions*, *5*(3), 351–368. https://doi.org/10.5194/os-5-351-2009

Rummelhart, D. E. (1986). Learning representations back-propagating errors. *Nature*, *323*(9), 533–536.

Schade, L. R., & Emanuel, K. A. (1999). The ocean's effect on the intensity of tropical cyclones: Results from a simple coupled atmosphere-ocean model. *Journal of the Atmospheric Sciences*, *56*(4), 642–651. https://doi.org/10.1175/1520-0469(1999)056%3C0642:TOSEOT%3E2.0.CO;2

Shchepetkin, A. F., & McWilliams, J. C. (2005). The Regional Oceanic Modeling System (ROMS): A split-explicit, free-surface, topography-following-coordinate oceanic model. *Ocean Modelling*, *9*(4), 347–404. https://doi.org/10.1016/j.ocemod.2004.08.002

Skamarock, W. C., Klemp, J. B., Dudhia, J., Gill, D. O., Barker, D. M., Duda, M. G., et al. (2008). A description of the Advanced Research WRF version 3, NCAR technical note, Mesoscale and Microscale Meteorology Division. Boulder, CO: National Center for Atmospheric Research.

Vincent, E. M., Lengaigne, M., Madec, G., Vialard, J., Samson, G., Jourdain, N. C., et al. (2012). Processes setting the characteristics of sea surface cooling induced by tropical cyclones. *Journal of Geophysical Research*, *117*, C02020. https://doi.org/10.1029/2011JC007396

Warner, J. C., Armstrong, B., He, R., & Zambon, J. B. (2010). Development of a coupled ocean-atmosphere-wave-sediment transport (COAWST) modeling system. *Ocean Modelling*, *35*(3), 230–244. https://doi.org/10.1016/j.ocemod.2010.07.010

Wei, J., Jiang, G., Liu, X., & Wang, H. (2017). Parameterization of typhoon-induced ocean cooling using temperature-equation and machine-learning algorithms: An example of typhoon Soulik (2013). *Ocean Dynamics*, *67*(9), 1179–1193. https://doi.org/10.1007/s10236-017-1082-z

Wei, J., Malanotte-Rizzoli, P., Eltahir, E. A. B., Xue, P., & Xu, D. (2014). Coupling of a regional atmospheric model ($RegCM_3$) and a regional ocean model (FVCOM) over the Maritime Continent. *Climate Dynamics*, *43*(5-6), 1575–1594. https://doi.org/10.1007/s00382-013-1983-3

Wei, J., Wang, D., Li, M., & Rizzoli, P. (2014). Coupled seasonal and intraseasonal variability in the South China Sea. *Climate Dynamics*, *44*, 2463–2477.

Zeng, X., & Beljaars, A. (2005). A prognostic scheme of sea surface skin temperature for modeling and data assimilation. *Geophysical Research Letters*, *32*, L14605. https://doi.org/10.1029/2005GL023030

Zhu, T., & Zhang, D.-L. (2006). The impact of the storm-induced SST cooling on hurricane intensity. *Advances in Atmospheric Sciences*, *23*(1), 14–22. https://doi.org/10.1007/s00376-006-0002-9